ELSEVIER

Catalysis Today 67 (2001) 65–75

CATALYSIS TODAY

www.elsevier.com/locate/cattod

The partial oxidation of methane to syngas in a palladium membrane reactor: simulation and experimental studies

Angelo Basile*, Luca Paturzo, Fortunato Laganà

Research Institute on Membranes and Modelling of Chemical Reactors, IRMERC-CNR, c/o University of Calabria, Via P. Bucci, Cubo 17/C, I-87030 Arcavacata di Rende (CS), Italy

Abstract

Among numerous potential applications of inorganic membrane reactors, the partial oxidation of methane (POM) may offer an alternative route, with respect to steam reforming of methane, for producing synthesis gas.

Inorganic membrane reactors are considered to be multifunctional reactors because they are able to combine catalytic reactions with membrane separation properties. In particular, dense palladium membranes are characterised by the fact that: (1) only hydrogen might permeate through them; (2) both Arrhenius and Sievert laws are followed.

In this investigation, a dense palladium membrane reactor (PMR) concept is analysed referring both to experimental data and to simulation study. The partial oxidation of methane (POM) reaction to produce synthesis gas was chosen as a model reaction to be investigated.

A membrane reactor model that includes the membrane, the gas phase and the catalyst activity is proposed. The experimental results in terms of methane conversion obtained by using a pin-hole free palladium membrane permeable to hydrogen only were compared with model predictions. The effect of reaction temperature on methane conversion at different time factors and sweep gas flow rates was considered. In particular, the effects of temperature profiles on the methane conversion are taken into account in the kinetic model.

Keywords: Partial oxidation of methane; Palladium membrane reactor; Syngas

1. Introduction

Energy availability is the first condition for high level development in human society. The most important challenge for all scientists is to find new energy sources and to optimise the traditional ones.

The new possible energy sources are nuclear energy (hot fusion), wind energy, solar and geothermal ones, while the traditional energy sources consist of fossil fuels and nuclear energy from fission. Since petroleum reservoirs seem to be insufficient for the next century, natural gas can be exploited in the next future as a primary energy source.

Natural gas consists of a gas mixture containing mainly methane, and it is utilised for producing synthesis gas (or syngas), i.e. a gas combination of H_2 and CO useful for many industrial productions. Syngas is an important starting material for several productions: ammonia and aldehydes, methanol and higher alcohols, and so on.

Nowadays, syngas can be produced from methane by means of three possible processes:

- Steam reforming : methane + steam → syngas
- Dry reforming : methane + carbon dioxide → syngas
- Partial oxidation : methane + oxygen → syngas

* Corresponding author. Tel.: +390-984-492011; fax: +390-984-402103.
E-mail address: basile@irmerc.cs.cnr.it (A. Basile).

0920-5861/01/$ – see front matter
PII: S0920-5861(01)00266-8

The first and the second reactions are endothermic ones (they need heat), while the third one is exothermic and methane conversion is always close to thermodynamic limitations.

If it is possible to remove one of the produced gases from the reaction system, methane conversion can increase with respect to the traditional processes. A dense palladium membrane reactor (PMR) is able to work in this way. In fact, it combines the typical characteristics of chemical reactions with the separating properties of palladium membrane, which is selectively permeable only to hydrogen gas. So, by removing the hydrogen produced through the membrane, methane conversion will increase.

The partial oxidation of methane (POM) reaction to produce synthesis gas was chosen as a model reaction to be investigated.

The possible reactions involved in this process are the following [1]:

1. $CH_4 + 2O_2 \Leftrightarrow CO_2 + 2H_2O$ (total combustion of methane)
2. $CH_4 + H_2O \Leftrightarrow CO + 3H_2$ (steam reforming reaction)
3. $CH_4 + 2H_2O \Leftrightarrow CO_2 + 4H_2$ (steam reforming reaction)
4. $CO + H_2O \Leftrightarrow CO_2 + H_2$ (water gas shift reaction)
5. $CH_4 + CO_2 \Leftrightarrow 2CO + 2H_2$ (dry reforming of methane)
6. $2CO \Leftrightarrow C + CO_2$ (Boudouard reaction)
7. $CH_4 \Leftrightarrow C + 2H_2$ (methane cracking)
8. $C + H_2O \Leftrightarrow CO + H_2$ (carbon gasification by steam)
9. $C + O_2 \Leftrightarrow CO_2$ (carbon gasification by O_2)

The H_2/CO ratio of the outlet stream of the process can be adjusted by means of the CH_4/O_2 feed ratio. In this work, a dense PMR is analysed for the POM to syngas with respect to both experimental data and simulation study.

2. Description of the process

2.1. Experimental

2.1.1. Traditional and membrane reactors

Traditional reactor (TR) consists of a stainless steel tube, length = 25 cm, i.d. = 0.67 cm. PMR consists of a stainless steel module containing a pin-hole free palladium membrane permeable to hydrogen only (furnished by ENEA, Italy), having thickness = 70×10^{-6} m, o.d. = 1.02 cm, length = 14 cm, with an internal movable ceramic support.

2.1.2. Experimental details

For both traditional and membrane reactors, the same experimental conditions were used. In particular, the lumen of both reactors was packed with catalyst particles Ni-5256 E 3/64 in. (furnished by Engelhard), catalyst weight = 3.12 g.

A schematic diagram of the experimental equipment is given in Fig. 1. The analysis is developed considering a PMR fed with a feed ratio of $CH_4/O_2/N_2 = 2/1/14$, methane feed stream $= 2 \times 10^{-3}$ mol/min, operating in a co-current flow configuration (with N_2 as sweep gas). According to Kikuchi and Chen [2], POM results from an initial reaction of complete combustion of a part of methane (reaction 1) which consumes all the oxygen. Then the produced water vapour and carbon dioxide are reduced by the residual methane or hydrogen (reactions 2,3,5).

The same feed conditions were used for the TR (except for sweep gas, of course). The catalytic bed was pre-treated using N_2 with a flow rate of 1.02×10^{-3} mol/min for 6 h at 480°C.

Gases used in the permeation tests for membrane reactor were nitrogen and hydrogen; this membrane was characterised with both Arrhenius and Sievert plots. All gases used were >99.995% pure. Methane conversion and hydrogen selectivity for membrane reactor were calculated referring to both permeate and retentate flows; water as product was removed by means of water-traps (condensers) and adsorbent columns containing drierite, furnished by the W.A. Hammond Drierite. Each stream was analysed using a Carlo Erba 4200 Gas Chromatograph, containing a stainless steel packed column Carboxen™ 1000, with oven temperature of 140°C and carrier gas flow rate (argon) of 25 ml/min. The detector used is a TCD at 250°C.

During reaction tests, the pressure ranged between 0.2 and 0.6 bar rel, while temperature ranged between 250 and 550°C (set point). For each reactor, two independent thermocouples were located at both ends of the modules: the first (feed side) was connected to a temperature controller (set point), while the second

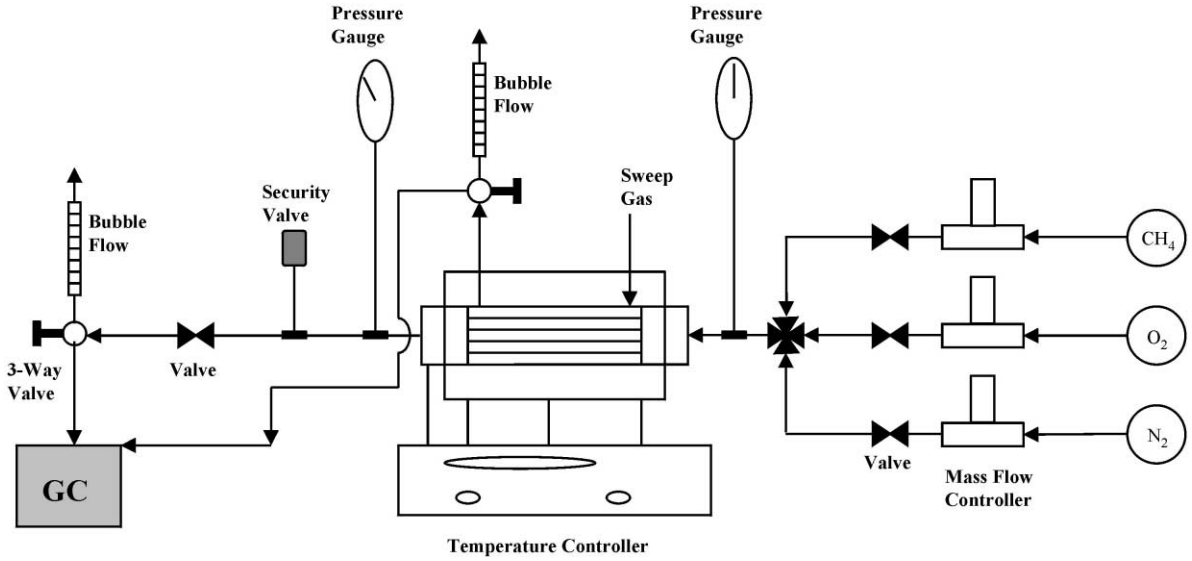

Fig. 1. Experimental apparatus.

was used to verify the temperature value at the retentate side for membrane reactor, and at the lumen outlet for TR. The maximum temperature difference was 1°C. Moreover, a 4-point movable thermocouple was used in order to measure temperature profiles inside both traditional and membrane reactors.

2.2. Simulation

2.2.1. Dynamic equilibrium

At first, the reaction system is considered not limited by chemical kinetics and thus the feed gas is assumed to be continuously at equilibrium throughout the PMR. As hydrogen permeates through the palladium layer and temperature profile changes, the feed gas composition changes due to hydrogen permeation and different equilibrium temperature. This means that the reaction rate is not the limiting step. All molecules in contact with the catalyst react with an infinite velocity. For a TR, the concentrations of species are a function of thermodynamic equilibrium resulting from an adiabatic heat balance inside the reactor. For the PMR, the fluidodynamic of the system must be considered because of hydrogen permeation that changes the equilibrium compositions. This condition is named "dynamic equilibrium". This model was developed using all the thermodynamic values for the reaction species; hydrogen removal was calculated using experimental permeabilities (Arrhenius plot). The resulting equilibrium is due to both adiabatic heat balance and fluidodynamic phenomena.

2.2.2. Simulation model

In this section, we outline the simulation of the catalytic POM into synthesis gas in a one-dimensional model for both TR and PMR. Temperature and concentration gradients are taken into account in axial direction only. The gradients over the fluid film surrounding the catalyst pellet are considered negligible. Deactivation by carbon deposition is not taken into account in the simulations.

The axial differential mass balance, in terms of molar flow rate for each chemical species, gives the following set of ordinary differential equations:

$$\frac{\mathrm{d}F_{\mathrm{CH_4}}}{\mathrm{d}W} = -\eta_1 v_1 - \eta_2 v_2 - \eta_4 v_4,$$

$$\frac{\mathrm{d}F_{\mathrm{O_2}}}{\mathrm{d}W} = -2\eta_1 v_1, \quad \frac{\mathrm{d}F_{\mathrm{H_2}}}{\mathrm{d}W} = 3\eta_2 v_2 + \eta_3 v_3 + 4\eta_4 v_4,$$

$$\frac{\mathrm{d}F_{\mathrm{CO}}}{\mathrm{d}W} = \eta_2 v_2 - \eta_3 v_3, \quad \frac{\mathrm{d}F_{\mathrm{CO_2}}}{\mathrm{d}W} = \eta_1 v_1 + \eta_3 v_3 + \eta_4 v_4,$$

$$\frac{\mathrm{d}F_{\mathrm{H_2O}}}{\mathrm{d}W} = 2\eta_1 v_1 - \eta_2 v_2 - \eta_3 v_3 - 2\eta_4 v_4, \quad \frac{\mathrm{d}F_{\mathrm{N_2}}}{\mathrm{d}W} = 0$$

The boundary conditions are:

for $W = 0$,

$$F^0_{CH_4} = 1.6667 \times 10^{-5}, \quad F^0_{O_2} = 3.334 \times 10^{-5},$$
$$F^0_{CO} = 0, \quad F^0_{CO_2} = 0, \quad F^0_{H_2} = 0, \quad F^0_{H_2O} = 0,$$
$$F^0_{N_2} = 2.334 \times 10^{-4}$$

where F_i is the molar flow rate for the species i (mol/s); W the mass of the catalyst (kg); η_j the effectiveness factor for the reaction j (–); v_j the rate equation for the reaction j (mol/(s kg_{cat})).

The energy equation is

$$F_{tot}\, cp_s \frac{dT}{dW} = \sum_{j=1}^{4} \eta_j v_j (-\Delta H_j) - Q_0$$

The boundary condition is:

for $W = 0$,

$$T^0 = \text{set point temperature}$$

where F_{tot} is the total molar flow rate (mol/s); cp_s the average specific heat of the gas mixture (J/(mol K)); ΔH_j the heat of the reaction j (J/mol); Q_0 the heat furnished to the reaction system (J/(s kg_{cat})).

Pressure drop equation was not considered, since the maximum pressure drop along the reactor was 0.02 bar.

In particular, the heat furnished to the reaction system (Q_0) is related to both the temperature profile along the reactor and the set point temperature of the reactor. The effectiveness factors are generally obtained from the integration of the second order differential equations describing the evolution of the different species inside the catalyst pellet [3]. These coefficients are related to a particular fluidodynamic condition because they take into account the mass transfer resistances inside and outside the catalyst (due to molecules diffusion). Generally, effectiveness factors depend on both temperature and total flow rate of the gas mixture. In this work, they have been considered as calibration parameters and their value has been calculated matching experimental data. However, since in our reaction system the total combustion (reaction 1) is the most important one from an energetic point of view, the effectiveness factor related to this reaction should be more incisive than the effectiveness factors related to the other reactions.

The simulation model applied to the dynamic equilibrium condition takes into account an average temperature between the set point temperature and the theoretical adiabatic temperature for the POM reaction. This average temperature is calculated considering the parabolic theoretical profile of the temperature along the reactor. Vice versa, the simulation that takes into account kinetics expressions includes le temperature profiles along the reactor.

2.2.3. Kinetic model and kinetic equations

Kinetic equations [1] and kinetic coefficients [4,5] of the reaction system were considered. In particular, among the nine reactions reported, only the first four were considered. The coke formation is negligible because of high catalyst stability and lower temperature with respect to traditional operations. The differential equations resulted from both the mass and energy balances were integrated with a Runge–Kutta algorithm of the fourth order. A comparison between experimental results for PMR and simulation results led to the determination of the effectiveness values for the four considered reactions.

According to Dissanayake et al. [6], in the reactor in which POM is carried out over a Ni/Al_2O_3 catalyst, there are three different catalytic zones:

- In the first one, there is a $NiAl_2O_4$ phase with moderate activity for total oxidation of methane to CO_2 and H_2O.
- In the second one, the catalyst consists of NiO and Al_2O_3 and it shows high activity for total oxidation.
- In the third one, metallic Ni is present and H_2 and CO are produced.

In this way, steam reforming is consecutive to total oxidation of methane; this phenomenon has been included in the kinetic model [1].

3. Results and discussion

3.1. Permeation tests: Sievert and Arrhenius plots

The membrane shows infinite selectivity H_2/N_2. Fig. 2 shows the Sievert plot for the dense PMR at different values of temperature: hydrogen flux increases with increasing difference in square roots of the partial pressure of hydrogen on the high and low pressure

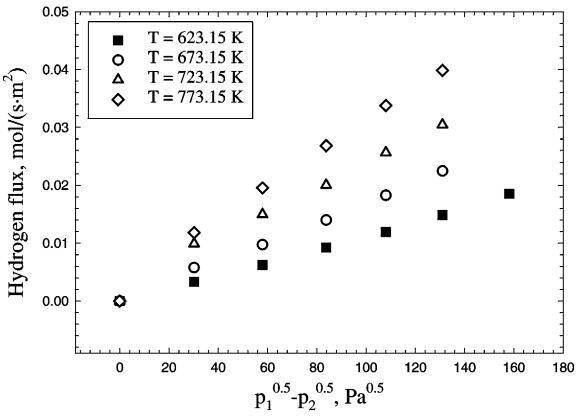

Fig. 2. Hydrogen flux versus difference in square roots of the partial pressure of hydrogen on the high and low pressure sides for different temperatures (Sievert plot for PMR).

sides ($\sqrt{p_1} - \sqrt{p_2}$). The behaviour of hydrogen flux versus temperature at various Δp ($p_1 - p_2$) is reported in Fig. 3: higher Δp corresponds to higher hydrogen fluxes. An Arrhenius plot of ln(Pe), where Pe is the permeability of pure hydrogen through the palladium membrane, versus $1000/T$ gives a linear relationship (Fig. 4). The apparent activation energy from these data is $E_a = 29.73\,\text{kJ/mol}$, while the pre-exponential factor is $\text{Pe}_0 = 7.7 \times 10^{-5}\,\text{mol m/(s m}^2\,\text{kPa}^{0.5})$.

Similar results for the permeation of hydrogen through dense palladium membranes are presented in Table 1. In particular, it is evident that the relative magnitude of both the apparent activation energy and

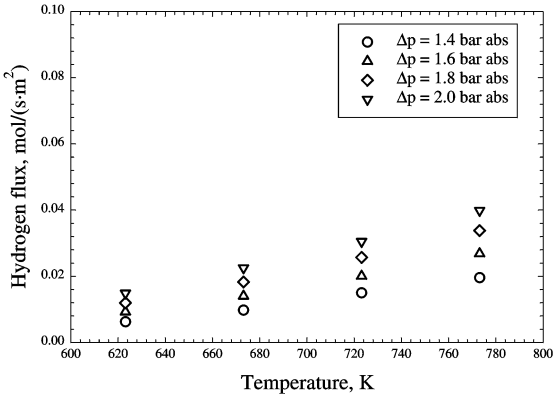

Fig. 3. Hydrogen flux versus temperature for different partial pressure of hydrogen differences on the high and low pressure sides (PMR).

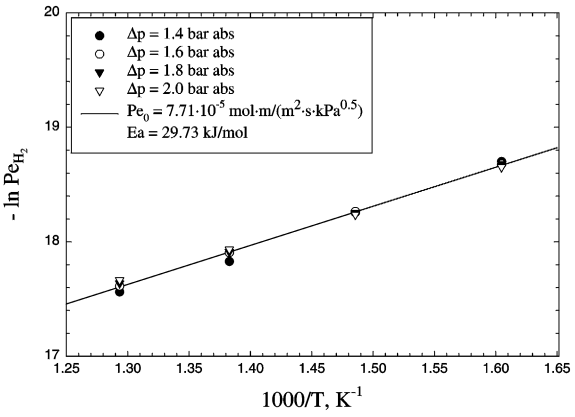

Fig. 4. Arrhenius plot for PMR.

the pre-exponential factor obtained in this study are similar to data in the literature [7–11].

3.2. Effect of temperature cycles on methane conversion

Fig. 5 shows the behaviour of methane conversion versus temperature for both TR and PMR. For both TR and PMR, the reaction was carried out starting from the ambient temperature to 300°C and afterwards increasing temperature at 50°C steps with holding times of 30 min. In particular, for TR, increasing temperature from ambient temperature to 300°C and afterwards to 550°C, methane conversion is 0% until $T = 450$°C, because the catalyst was not activated and the reaction occurred only at $T = 500$°C, with a methane conversion of 35.5%; the maximum methane conversion (47.5%) was reached at 550°C. As shown in Fig. 5, in the cooling-down steps, the catalyst exhibited a different temperature dependence for methane conversion

Table 1
Apparent activation energy and pre-exponential factor from the literature

E_a (kJ/mol)	Pe_0 (10^{-5} mol m/(s m^2 kPa$^{0.5}$))	Reference
29.73	7.71	This work
15.70	2.19	Koffler et al. [7]
15.50	2.54	Balovnev [8]
12.48	0.38	Itoh and Xu [9]
18.45	1.02	Itoh et al. [10]
48.50	9.33	Tosti et al. [11]

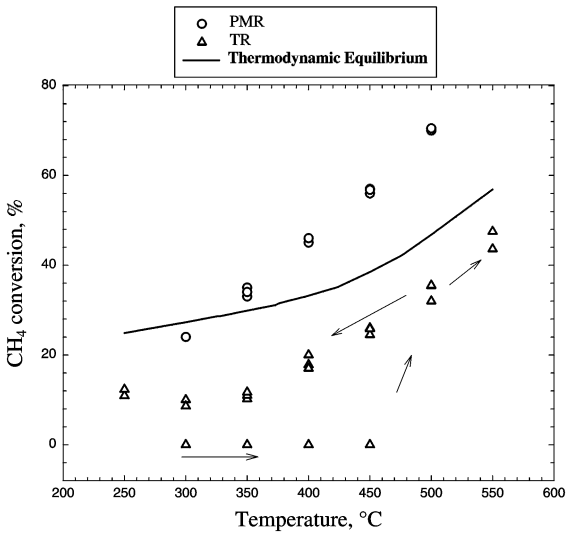

Fig. 5. Methane conversion versus temperature for TR and PMR. Experimental conditions: $CH_4/O_2/N_2 = 2/1/14$, $CH_{4,in} = 2 \times 10^{-3}$ mol/min, $P_{in} = 1.6$ bar abs.

from the one of the fresh Ni-based catalyst shown in the heating-up stage. Decreasing temperature from 550 to 250°C, methane conversion reaches 11% at 250°C.

Moreover, increasing temperature again, starting from 250°C, the next cycle of sequential temperature changes does not produce any hysteresis phenomena meaning that Ni-based catalyst maintained the activation of the previous cycle.

Considering the POM reaction, the same hysteresis phenomena for the same reaction have been observed by Dissanayake et al. [6] using a Ni/Al_2O_3 catalyst, Dissanayake et al. [12] using a Ni/Yb_2O_3 catalyst, Chu et al. [13] using NiO/La_2O_3 catalyst, Boucouvalas et al. [14] using both Ru/TiO_2 and $Ru/\gamma\text{-}Al_2O_3$ catalysts, Nakagawa et al. [15] confirmed the phenomena for Ir/TiO_2 catalyst, and by Basile et al. [16] using the same Ni-based catalyst used in this work.

Vice versa, for PMR the hysteresis phenomenon was not observed, as shown in Fig. 5. In this case, for each temperature reaction, the temperature increasing from 300 to 500°C and the temperature decreasing from 500 to 300°C show the same values of methane conversion. This might be due, probably, to the fact that palladium itself acts as a catalyst for the methane oxidation. It is to be noted, in Fig. 5, that each experimental point for TR is always below the thermodynamic equilibrium curve for each reaction temperature, while for PMR methane conversion is above the corresponding thermodynamic values for $T > 300$°C.

3.3. Dynamic equilibrium

An investigation carried out using a mobile thermocouple showed the existence of a temperature profile inside both the PMR and the TR (see Fig. 6). For TR, the maximum temperature (527°C) was observed when the set point temperature was 500°C, without pre-heating the feed gas mixture. In the case of PMR, two different profiles are observed, depending on the pre-heating temperature of the feed stream. At $T_{feed} = 260$°C, the maximum temperature was 615°C, while at $T_{feed} = 380$°C, the maximum temperature was 656°C. As we expected, considering that POM results from an initial reaction of complete exothermal combustion of a part of methane, the maximum temperature is found close to the reactors inlet.

Fig. 7 shows experimental data on methane conversion versus temperature for both PMR and TR. Methane conversion for PMR is always higher than methane conversion for TR. This is due to the hydrogen that permeates selectively through the palladium shifting the equilibrium of the reaction towards products. In fact, methane conversion for PMR is for all the temperatures greater than 300°C above the thermodynamic equilibrium curve, while methane conversion for TR is always below the thermodynamic curve. In particular, at 300°C, methane conversion for PMR is 24 versus 9% for TR. At 300°C, the methane conversion for PMR is close to the thermodynamic value probably because of the relatively low permeability of the hydrogen through the palladium at this temperature. In the same figure, a curve representing the dynamic equilibrium simulation for methane conversion is also reported. Of course this curve, representing the ideal maximum methane conversion for our reaction system, is always the highest one. It is to be noted that dynamic equilibrium also depends on the hydrogen permeability (that is an exponential function of temperature).

Fig. 8 shows an increase in methane conversion with increasing sweep gas flow rate for PMR at 350°C. Experimental results obtained using PMR are above thermodynamic equilibrium values for

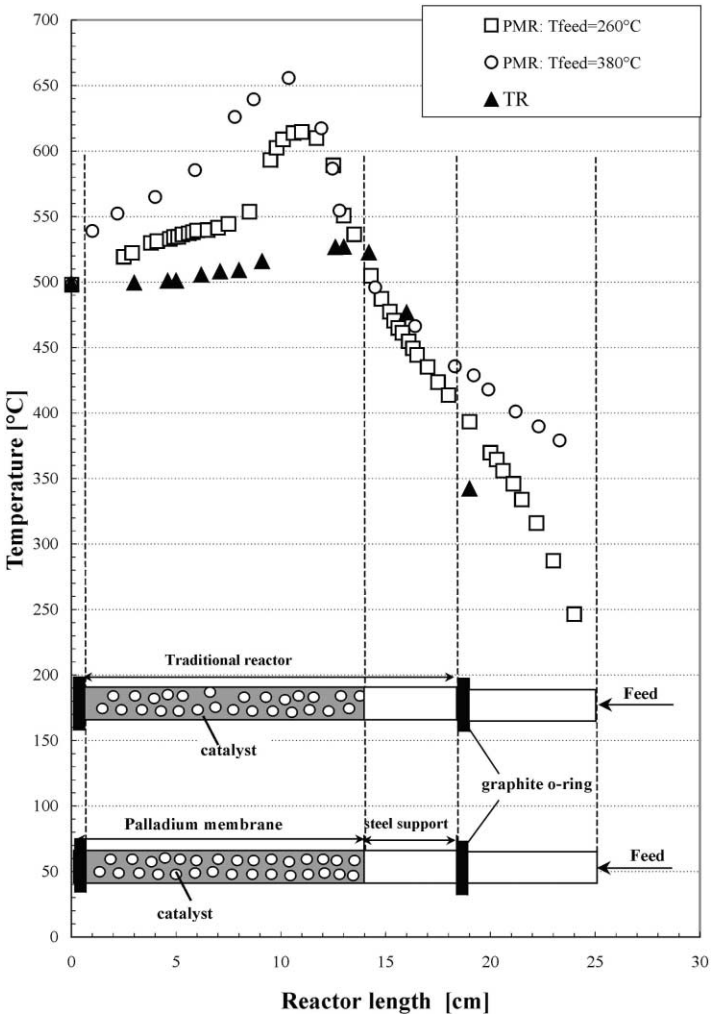

Fig. 6. Temperature profiles inside both TR and PMR.

$N_2 > 8 \times 10^{-3}$ mol/min and they tend to a constant methane conversion value (35%). This behaviour is quite expected. In fact, increasing the gas flow rate will increase the driving force that promotes hydrogen permeation. However, for high values of nitrogen sweep gas, the limiting step of the reaction is not yet the hydrogen removal. In other words, the rate of hydrogen removal becomes greater than the rate of hydrogen production. So, by increasing the sweep gas flow rate, the driving force reaches a maximum value corresponding to a hydrogen molar fraction, i.e. zero in the shell side.

In the same figure, for the same feed gas ratio $CH_4/O_2/N_2 = 2/1/14$, thermodynamic equilibrium calculated at 350°C is shown. PMR experimental data are close to thermodynamic equilibrium but quite far from dynamic equilibrium, that represents the maximum achievable methane conversion.

Methane conversion increases with increasing time factor, as shown in Fig. 9. In particular, in PMR methane conversion reaches 84% at $W/F = 4288\,g_{cat}\,min/mol_{CH_4}$, while for TR the maximum methane conversion is only 56% at $7630\,g_{cat}\,min/mol_{CH_4}$. For what concerns PMR, the maximum methane

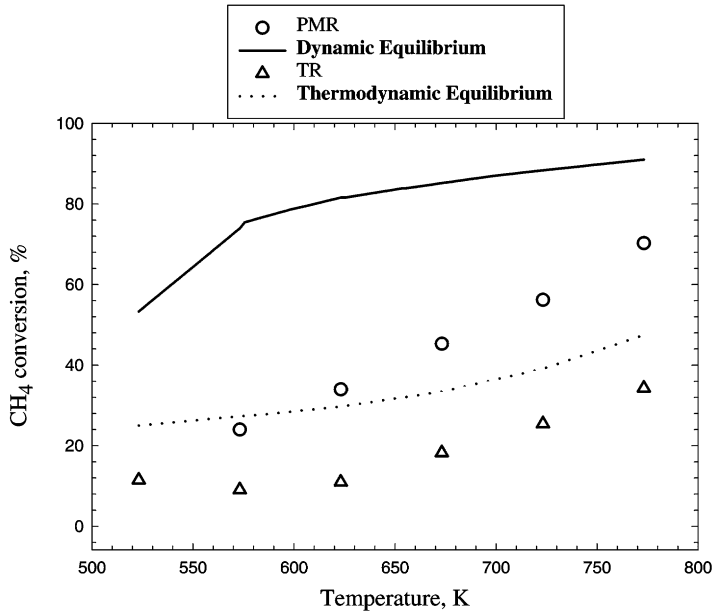

Fig. 7. Methane conversion versus temperature for TR and PMR: experimental data, dynamic and thermodynamic simulation results.

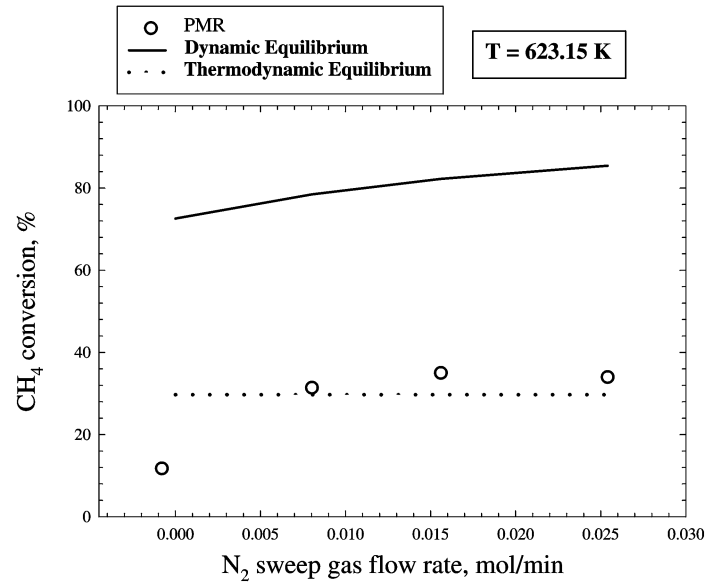

Fig. 8. Methane conversion versus sweep gas flow rate for PMR: experimental data, dynamic and thermodynamic simulation results.

conversion is 96% at 4288 g_{cat} min/mol_{CH_4} and at 823.15 K. To be observed that experimental data for PMR at 773.15 K are below the corresponding dynamic equilibrium curve.

Fig. 10 shows the behaviour of hydrogen selectivity versus time factor at 500°C. TR shows the lowest constant value (44%) at the same temperature for each time factor compared to the equilibrium value

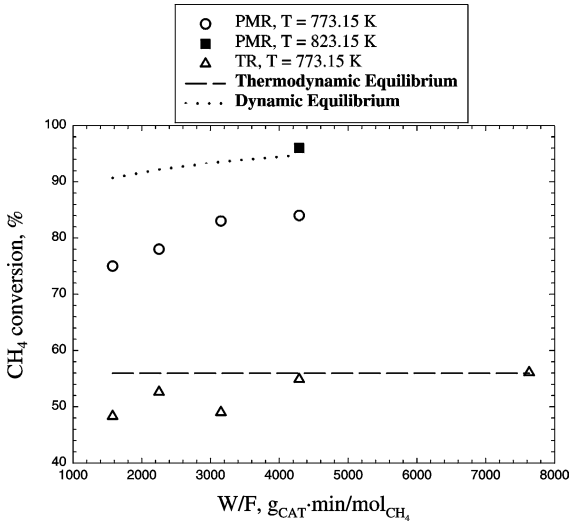

Fig. 9. Methane conversion versus time factor for TR and PMR. The conversion value of 96% related to a time factor of 4288 g_{cat} min/mol_{CH_4} is referred to $T = 550°C$; the other curves are referred to $T = 500°C$.

(73%). PMR shows hydrogen selectivity greater than equilibrium value only for time factor $>$ 2500 g_{cat} min/mol_{CH_4}, but lower than the corresponding dynamic equilibrium. The maximum experimental hydrogen selectivity was 88.3% at 550°C, against 83% corresponding to thermodynamic equilibrium referred to the same set point temperature.

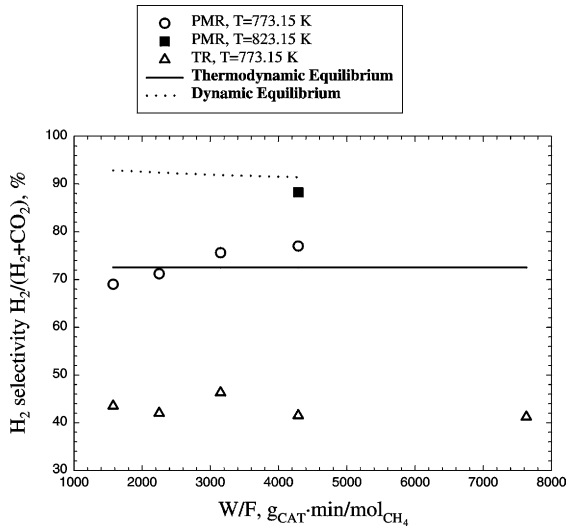

Fig. 10. Hydrogen selectivity versus time factor for TR and PMR. The selectivity value of 88% related to a time factor of 4288 g_{cat} min/mol_{CH_4} is referred to $T = 550°C$; the other curves are referred to $T = 500°C$.

3.4. Kinetic study

Four reactions were chosen among the possible ones that occur in the reaction system:

1. $CH_4 + 2O_2 \Leftrightarrow CO_2 + 2H_2O$ (total combustion of methane)
2. $CH_4 + H_2O \Leftrightarrow CO + 3H_2$ (steam reforming reaction)
3. $CH_4 + 2H_2O \Leftrightarrow CO_2 + 4H_2$ (steam reforming reaction)
4. $CO + H_2O \Leftrightarrow CO_2 + H_2$ (water gas shift reaction)

For each reaction, an effectiveness factor was considered. Their value depends on the experimental conditions. In fact, as reported in Section 2.2.2, these coefficients are related to a particular fluidodynamic condition because they take into account the mass transfer resistances inside and outside the catalyst (due to molecule diffusion), but in this work they have been considered as calibration parameters and their value has been calculated matching experimental data.

Fig. 11 shows the behaviour of the effectiveness factor versus the time factor for TR. The mass transfer coefficient changes with changing total flow rate. So, a change in the effectiveness factors is expected.

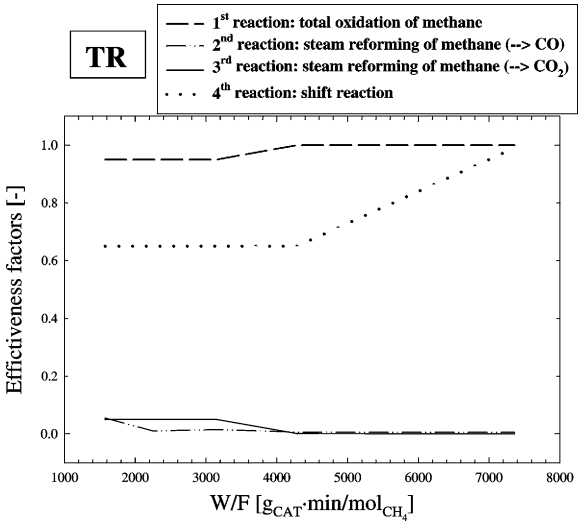

Fig. 11. Effectiveness factors versus time factor for TR, from kinetic simulation.

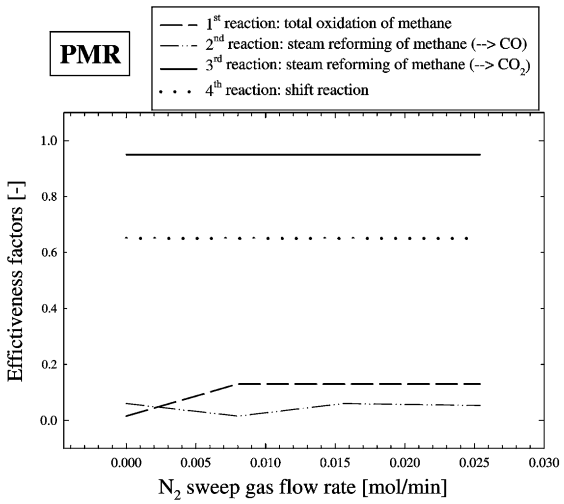

Fig. 12. Effectiveness factors versus sweep gas flow rate for PMR, from kinetic simulation.

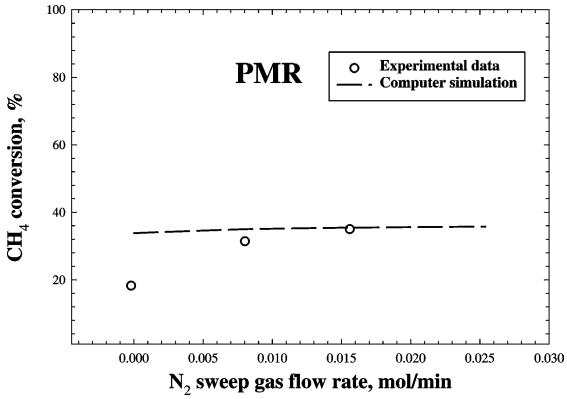

Fig. 13. Methane conversion versus nitrogen sweep gas for PMR at 623.15 K: experimental data and kinetic simulation results. The effectiveness factors are 0.13 (total oxidation), 0.06 (steam reforming $\rightarrow$ CO), 0.95 (steam reforming $\rightarrow$ CO_2), 0.65 (shift reaction).

However, it is possible to observe that among the above-mentioned four reactions, only the effectiveness factor of the water gas shift reaction changes significantly from 0.65 to 0.999. Moreover, with respect to PMR, effectiveness factors seem to depend only slightly on sweep gas flow rate, as shown in Fig. 12. In fact, since the flow rate of the reacting mixture is not changing, a very small change in the effectiveness factors is expected. Comparing Fig. 11 with Fig. 12, it can be observed that the effectiveness factor coupled to a particular reaction is generally quite different. This is also expected in PMR and not in TR, because the first one allows hydrogen to pass through the palladium changing the transport phenomena inside the reactor.

For PMR, for a fixed experimental setting of 350°C, feed pressure = 1.2 bar abs, time factor = 1574 g_{cat} min/mol_{CH_4}, feed ratio $CH_4/O_2/N_2 = 2/1/14$, CH_4 = 2×10^{-3} mol/min and sweep gas flow rate = 0.0156 mol/min, the effectiveness factors are the following:

1. Total combustion of methane : effectiveness factor = 0.13
2. Steam reforming reaction ($\rightarrow$ CO) : effectiveness factor = 0.06
3. Steam reforming reaction ($\rightarrow$ CO_2) : effectiveness factor = 0.95
4. Water gas shift reaction : effectiveness factor=0.65

Using these effectiveness factors, the simulation reported in Fig. 13 shows the comparison of methane conversion versus sweep gas flow rate in terms of both experimental data and simulation results. Methane conversion is well simulated only for $N_2 > 8 \times 10^{-3}$ mol/min, while the worst situation is obtained for $N_2 = 0$ mol/min. The simulation model fails in this condition, that presents a particular anomaly. In fact, the simulation calculates the hydrogen molar fraction in the shell side assuming the presence of nitrogen at 1 atm of total pressure. Assuming $N_2 = 0$ in the shell side means to consider one of the following possibilities: (1) there is a vacuum in the shell side; (2) there is H_2 in the shell side at 1 atm of total pressure. In the first case, the driving force for hydrogen is the maximum one, and it is necessary to consider a time dependency for the entire system. In the second case, vice versa, a counter-diffusion of hydrogen should be considered from the shell side to the lumen side in which the partial pressure of hydrogen in our experimental conditions is lower than 1 atm. In this last case, methane conversion will decrease.

4. Conclusions

The experimental studies carried out on the POM reaction show that it is possible to increase methane conversion values above the traditional equilibrium

ones using a PMR. The maximum methane conversion achieved using PMR was 96% at 550°C, time factor of 4288 g_{cat} min/mol_{CH_4}, $p = 1.2$ bar.

In order to interpret experimental results, a mathematical model for both dynamic simulation and kinetic simulation was developed. The model fits quite well experimental results for some experimental conditions. Particular attention should be paid to the dynamic equilibrium. In fact, it indicates whether the reactor should be improved in terms of operative conditions to approach better performances.

Acknowledgements

The authors wish to thank Dr. V. Violante (ENEA, Italy) for furnishing the palladium membrane, Engelhard Italiana S.p.A. (Italy) for furnishing the catalyst. Financial supports were provided both from CNR and Regione Calabria (POP 1994–1999, Sottoprogramma No. 4, Misura 4.4).

References

[1] A.M. De Groote, G.F. Froment, Appl. Catal. A 138 (1996) 245–264.
[2] E. Kikuchi, Y. Chen, Natural Gas Conversion V, Vol. 119, Elsevier, Amsterdam, 1998, pp. 441–446.
[3] O. Levenspiel, Ingegneria delle Reazioni Chimiche, Ambrosiana, Milano, 1978, p. 473.
[4] D.L. Trimm, C.-W. Lam, Chem. Eng. Sci. 35 (1980) 1405–1413.
[5] J. Xu, G.F. Froment, AIChE J. 35 (1) (1989) 88–96.
[6] D. Dissanayake, M.P. Rosynek, K.C.C. Kharas, J.H. Lunsford, J. Catal. 132 (1991) 117–127.
[7] S.A. Koffler, J.B. Hudson, G.S. Ansell, Trans. AIME 245 (1969) 1735–1740.
[8] Yu.A. Balovnev, Diffusion of hydrogen in palladium, Russ. J. Phys. Chem. 48 (1974) 409–410.
[9] N. Itoh, W.-C. Xu, Appl. Catal. A 107 (1993) 83–100.
[10] N. Itoh, W.-C. Xu, K. Haraya, J. Membr. Sci. 56 (1991) 315–325.
[11] S. Tosti, L. Bettinali, V. Violante, A. Basile, M. Chiappetta, A. Criscuoli, E. Drioli, C. Rizzello, in: Proceedings of the 20th Symposium on Fusion Technology, Marseille, France, September 7–11, 1998, pp. 1033–1036.
[12] D. Dissanayake, M.P. Rosynek, J.H. Lunsford, J. Phys. Chem. 97 (1993) 3644–3646.
[13] Y. Chu, S. Li, J. Lin, J. Gu, J. Yang, Appl. Catal. A 134 (1996) 67–80.
[14] Y. Boucouvalas, Z. Zhang, X.E. Verykios, Catal. Lett. 40 (1996) 189–195.
[15] K. Nakagawa, N. Ikenaga, T. Suzuki, T. Kobayashi, M. Haruta, Appl. Catal. A 169 (1998) 281–290.
[16] A. Basile, S. Fasson, G. Vitulli, E. Drioli, Natural Gas Conversion V, Vol. 119, Elsevier, Amsterdam, 1998, pp. 453–458.